Supporting Information

A simple colorimetric and ratiometric fluoride ion probe with large color change

Heng Shi, Hongjin Chen, Xiangguo Li, Jieni Xing, Gang Zhang, Rui Zhang, Jian Liu*

Jiangsu Co-Innovation Center of Efficient Processing and Utilization of Forest Resources, Jiangsu Key Lab of Biomass-based Green Fuels and Chemicals, College of Chemical Engineering, Nanjing Forestry University, Nanjing 210037, China.

*Corresponding author: Prof. Jian Liu, liu.jian@njfu.edu.cn

Table of contents

General.

Fig. S1 ^{1}H NMR spectra of compound **3** in $CDCl_3$-*d*.

Fig. S2 ^{13}C NMR spectra of compound **3** in $CDCl_3$-*d*.

Fig. S3 ^{1}H NMR spectra of compound **4** in $CDCl_3$-*d*.

Fig. S4 ^{13}C NMR spectra of compound **4** in $CDCl_3$-*d*.

Fig. S5 ^{1}H NMR spectra of probe **SHJ-1** in DMSO-d_6.

Fig. S6 ^{13}C NMR spectra of probe **SHJ-1** in DMSO-d_6.

Fig. S7 FT-IR spectrum of probe **SHJ-1**.

Fig. S8 ^{1}H NMR spectra of probe **SHJ-2** in DMSO-d_6.

Fig. S9 ^{13}C NMR spectra of probe **SHJ-2** in DMSO-d_6.

Fig. S10 FT-IR spectrum of probe **SHJ-2**.

Fig. S11 The stability of a) **SHJ-1** and b) **SHJ-2** in DMSO.

Fig. S12 The response time of a) **SHJ-1** and b) **SHJ-2** to F^- in DMSO solution.

Fig.S13 a) Absorption spectra of probe **SHJ-2** in DMSO with the addition of different equiv. of TBAF; b) The absorbace ratio (A_{302nm}/A_{380nm}) of **SHJ-2** versus F^- concentrations.

Fig. S14 a) Job's plot for complexation of **SHJ-2** with F^- anion. b) Benesi - Hildebrand plot of **SHJ-2** by UV-vis measurements. c) Absorbance of **SHJ-2** in the presence of TBAF at different concentration in DMSO.

Fig. S15 Absorbance spectra of **SHJ-2** in the presence of 23.33 equivalents of TBAF in DMSO with various content of water.

Fig. S16 The intensity of the maximum visible absorption peak of probes **SHJ-1** with the addition of 8 equiv. of various anions (as tetrabutylammonium salt) in a) DMF and b) DCM solution at room temperature. (Inset: Color changes of **SHJ-1** with the addition of 8 equiv. of various anions under ambient light). Absorption spectra of probe **SHJ-1** in c) DMF and d) DCM with the addition of different equiv. of TBAF;

Fig. S17 ^{1}H NMR titration spectra of the probe **SHJ-2** in DMSO-d_6 in presence of differernt equivalents of TBAF.

Fig. S18 The intensity of the maximum visible absorption peak of probes **SHJ-1** with the addition of 8 equiv. of various anions (as tetrabutylammonium salt) in a) DMF and b) DCM solution at room temperature.

Fig. S19 a) ^{1}H NMR titration spectra of the probe **SHJ-2** in DMSO-d_6 in presence of differernt equivalents of TBAF; b) Optimized structures of **SHJ-2** and **SHJ-2** + F^-.

Fig. S20 A schematic of probable complex formation reaction during the fluoride sensing process.

Table S1 Properties of **SHJ-1** and the reported acylhydrazone-based fluoride ion probes.

General

All chemicals and reagents were used as received from chemical companies without further purification unless otherwise stated. Column chromatography was performed using with silica gel as a stationary phase. Geometry optimization the pristine probes and binding with F^- were performed using B3LYP functional and 6-31G (d,p) basis set implemented in the Gaussian 16 program package.[1]

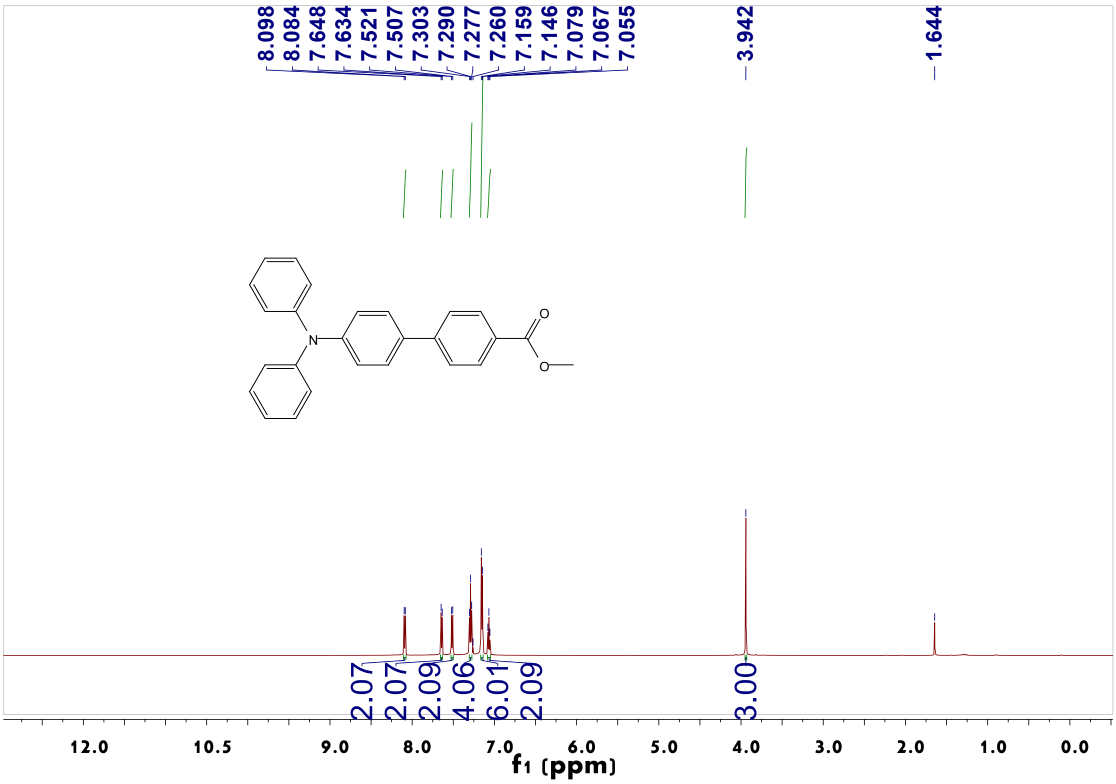

Fig. S1 ^{1}H NMR spectra of compound **3** in $CDCl_3$.

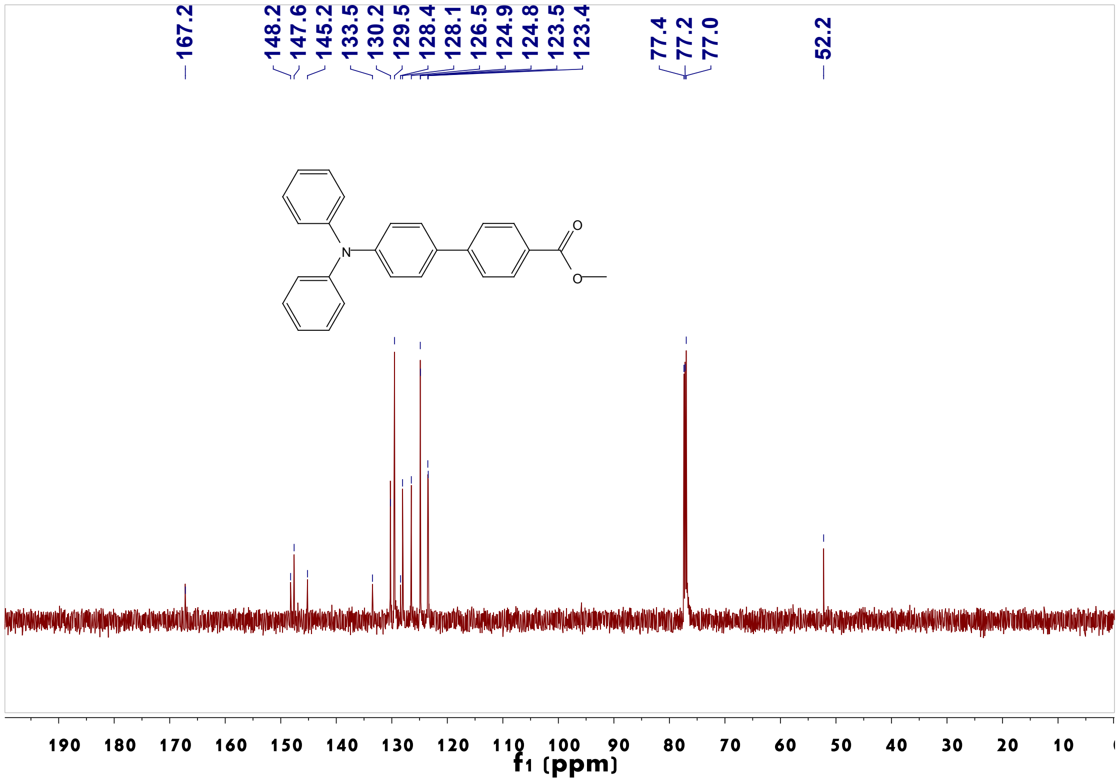

Fig. S2 ^{13}C NMR spectra of compound **3** in $CDCl_3$.

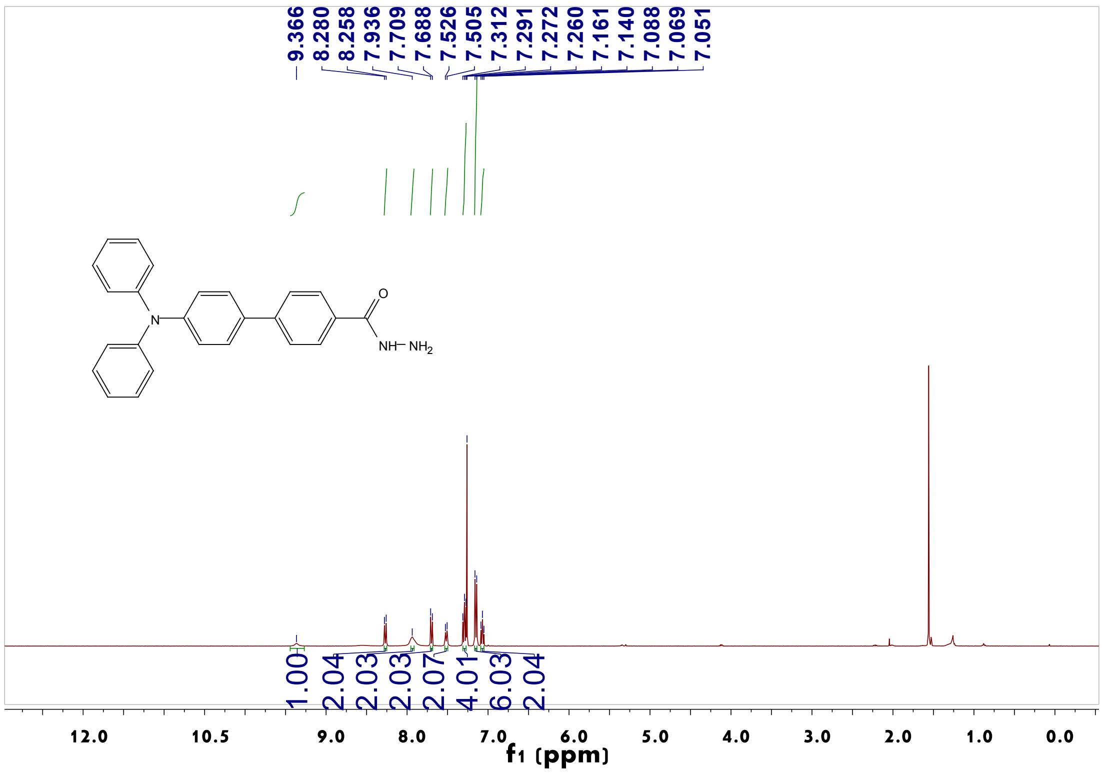

Fig. S3 ^{1}H NMR spectra of compound **4** in $CDCl_3$.

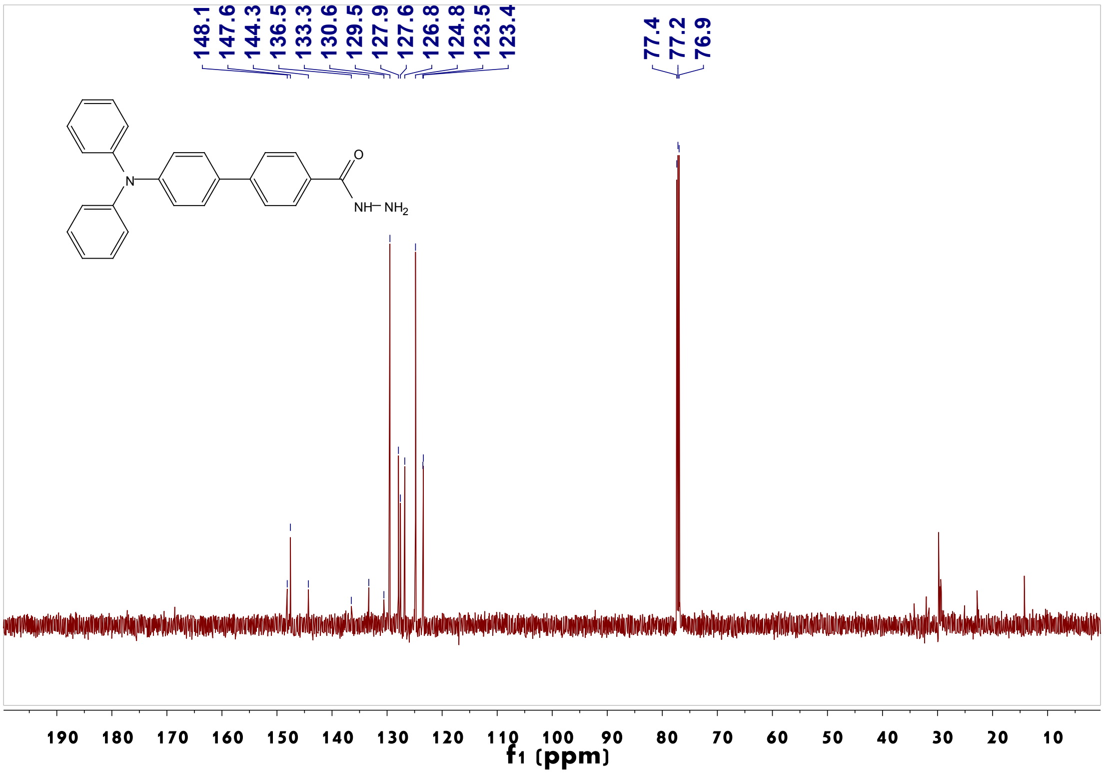

Fig. S4 ^{13}C NMR spectra of compound **4** in $CDCl_3$.

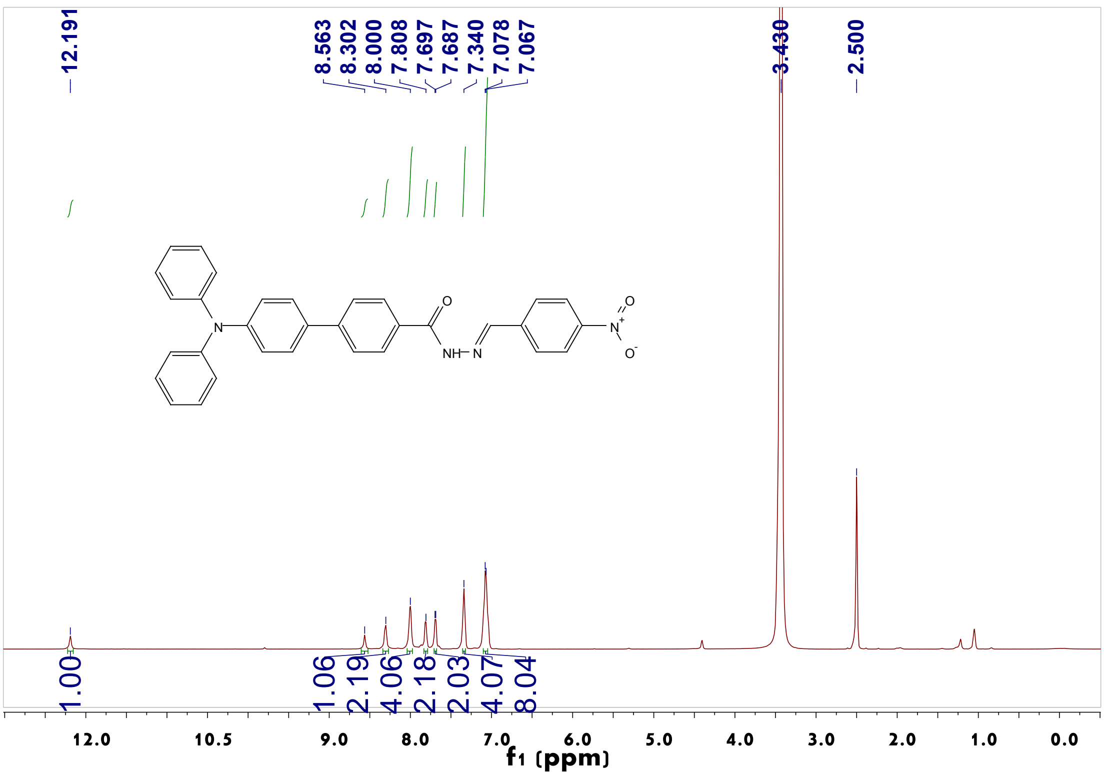

Fig. S5 ^{1}H NMR spectra of probe **SHJ-1** in DMSO-d_6.

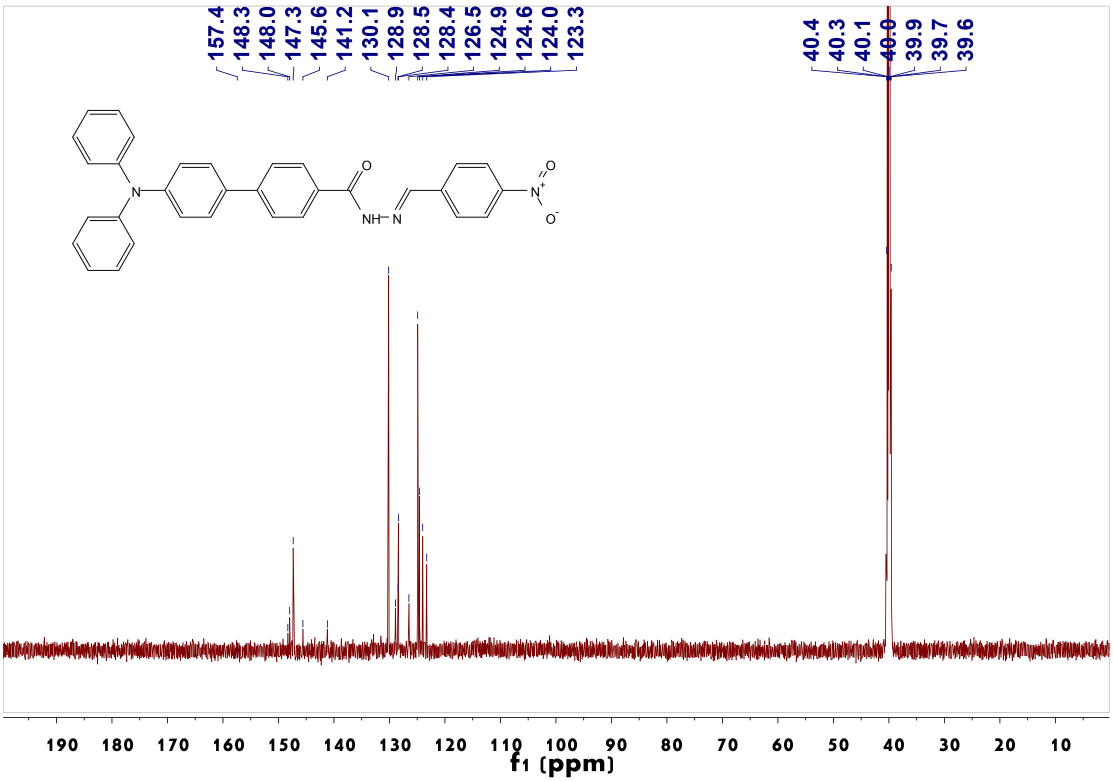

Fig. S6 ^{13}C NMR spectra of probe **SHJ-1** in DMSO-d_6.

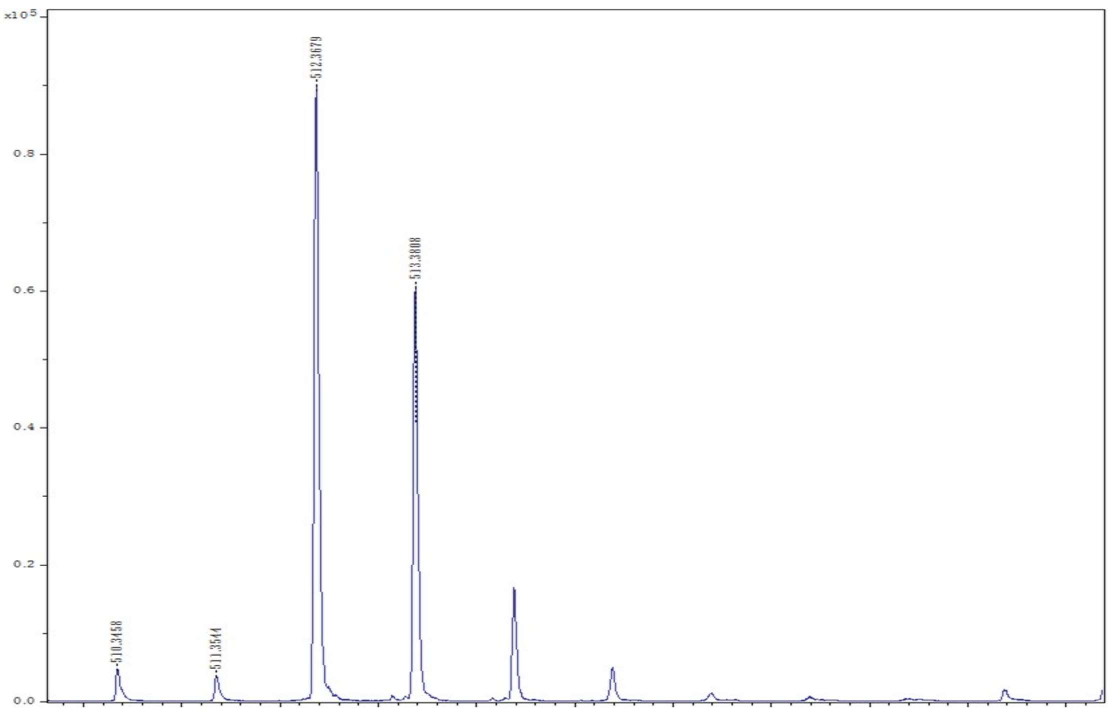

Fig. S7 Mass spectra of probe **SHJ-1**.

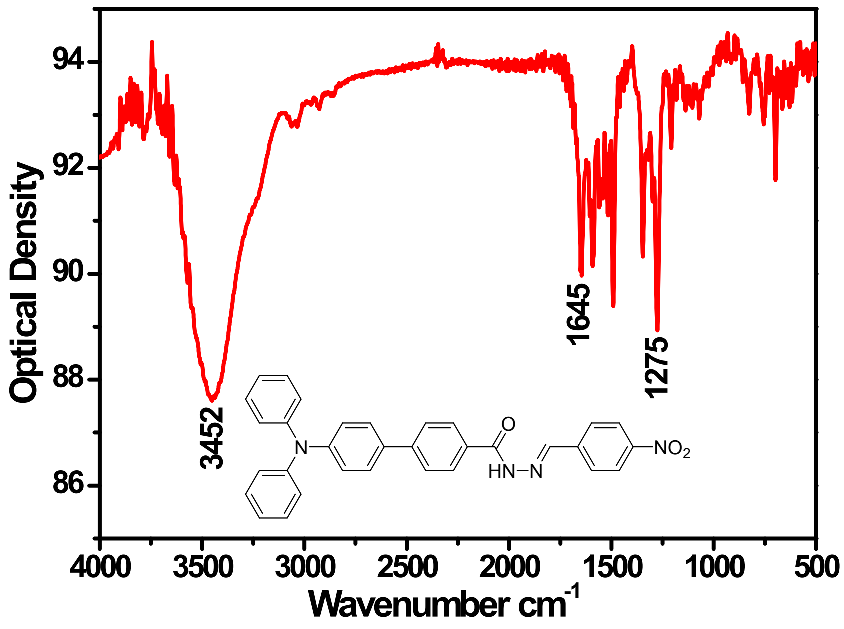

Fig. S8 FT-IR spectrum of probe **SHJ-1**.

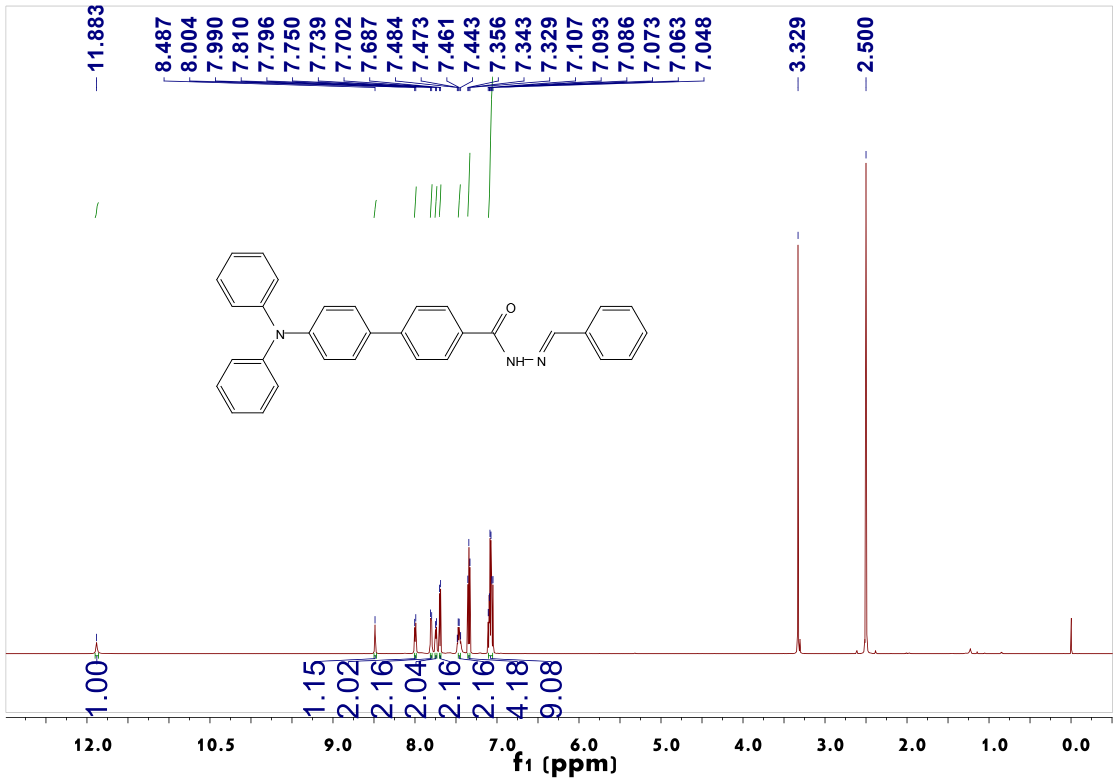

Fig. S9 ^{1}H NMR spectra of probe **SHJ-2** in DMSO-d_6.

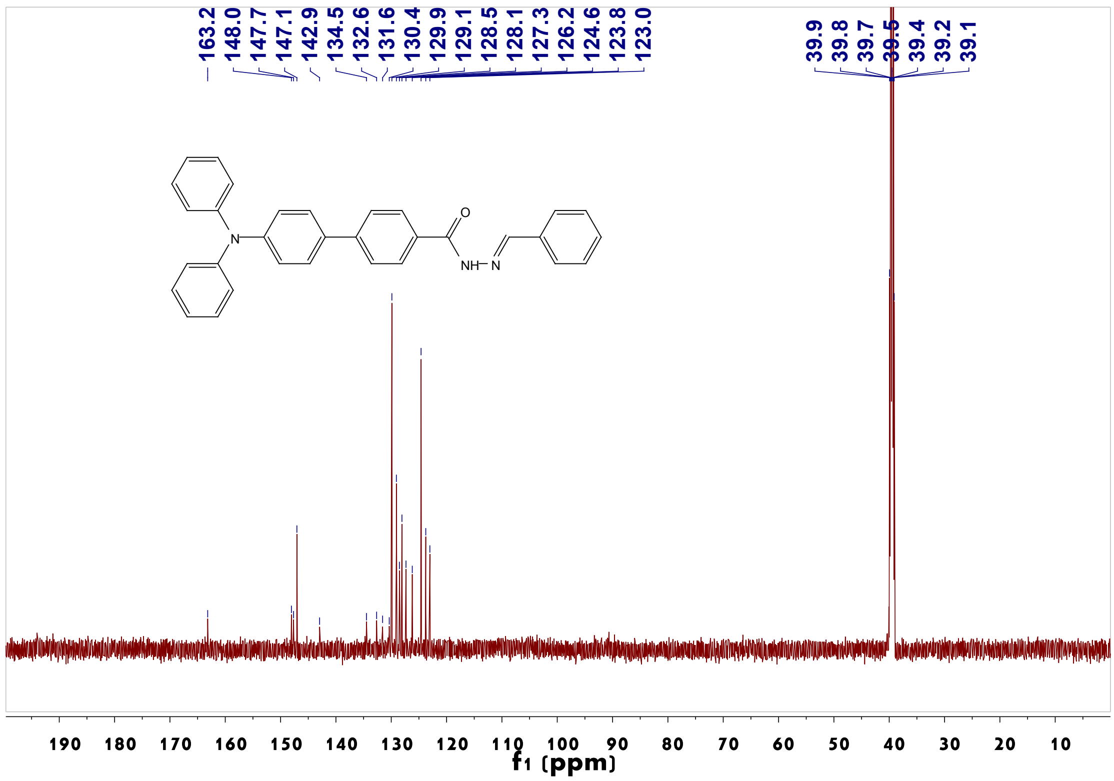

Fig. S10 [13]C NMR spectra of probe **SHJ-2** in DMSO-d_6.

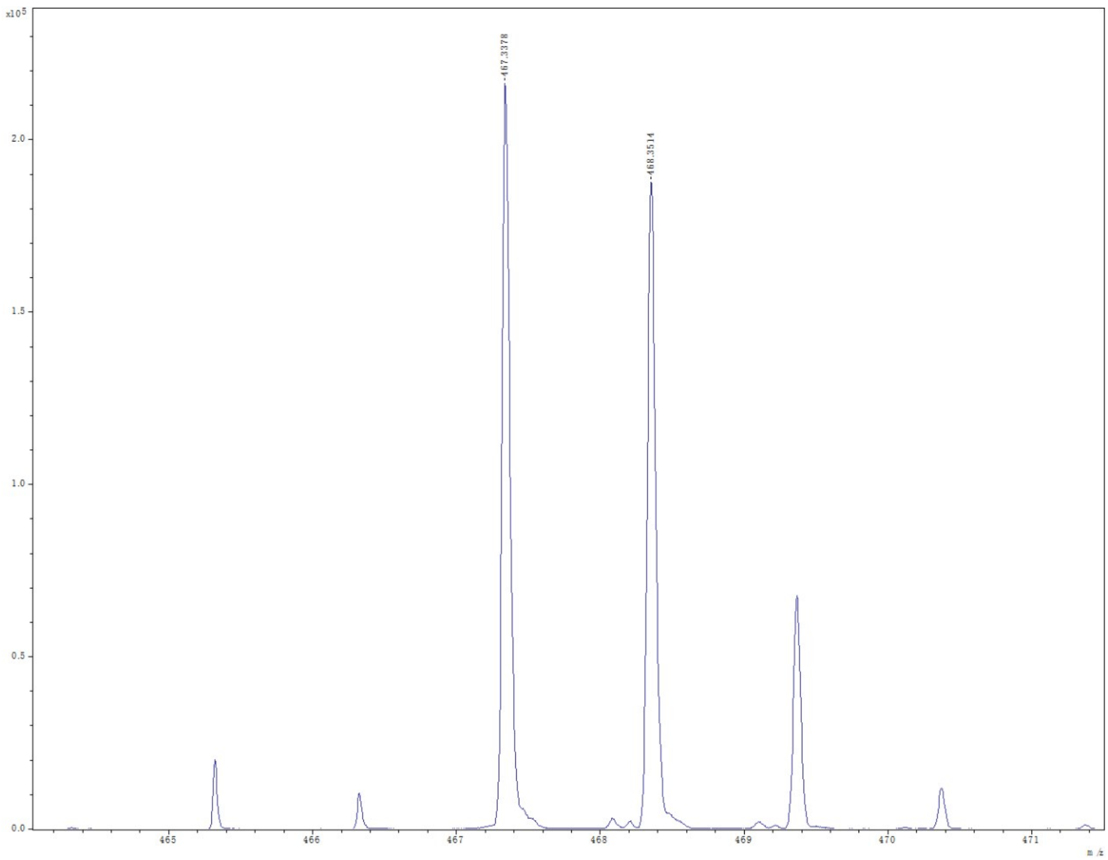

Fig. S11 Mass spectra of probe **SHJ-2**.

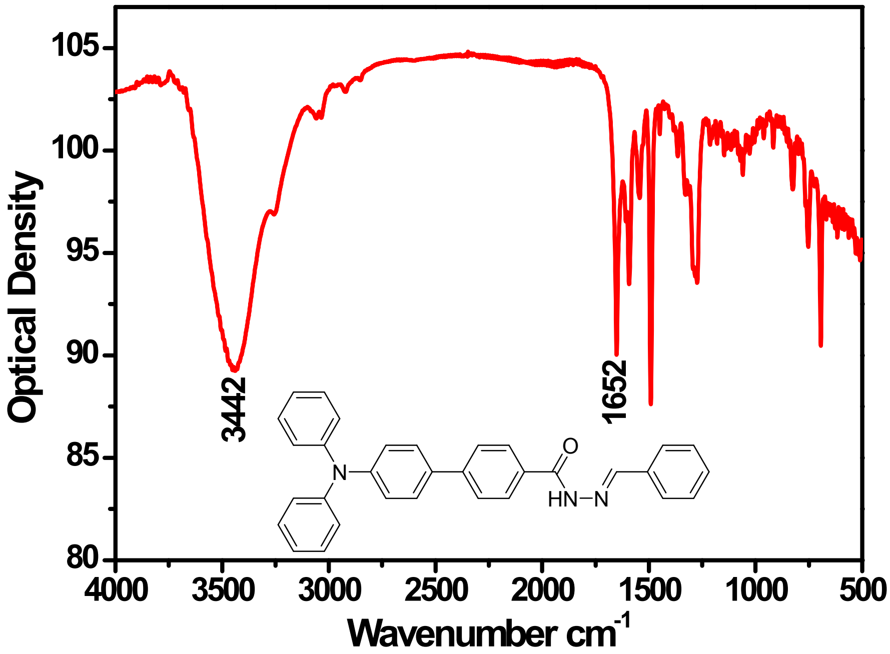

Fig. S12 FT-IR spectrum of probe **SHJ-2**.

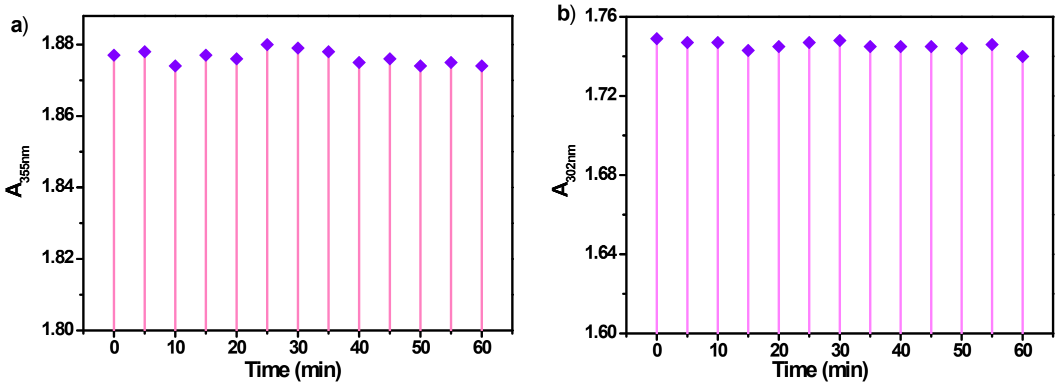

Fig. S13 The stability of a) **SHJ-1** and b) **SHJ-2** in DMSO.

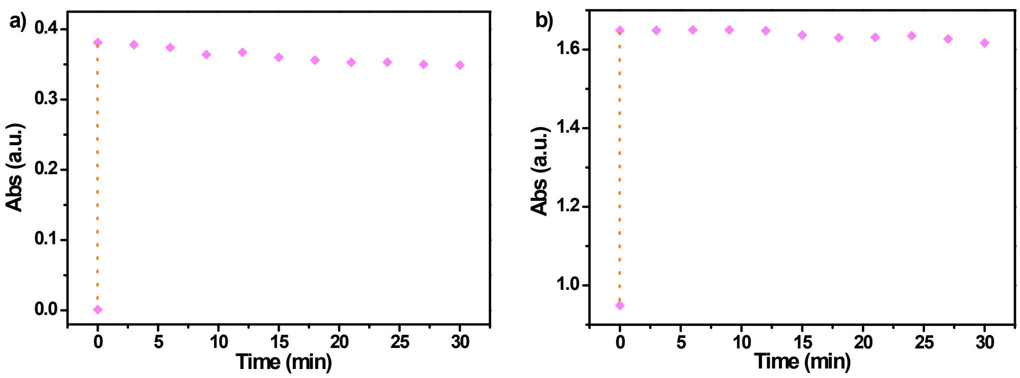

Fig. S14. The response time of a) **SHJ-1** and b) **SHJ-2** to F^- in DMSO solution.

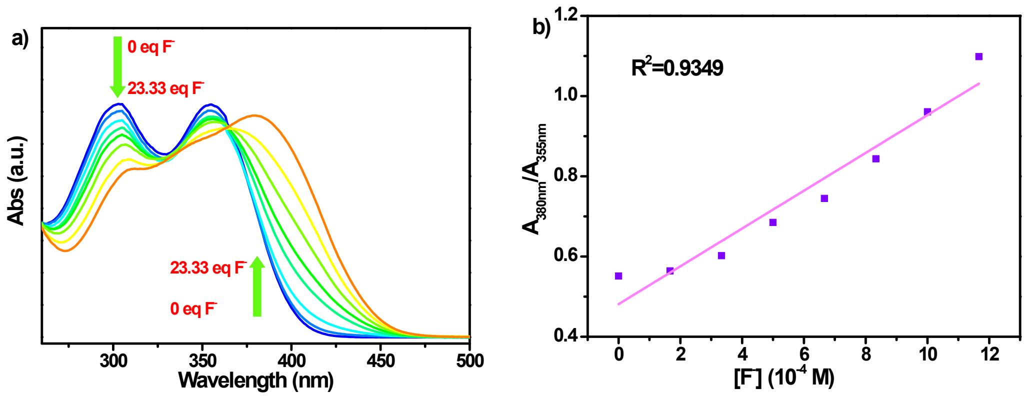

Fig. S15. a) Absorption spectra of probe **SHJ-2** in DMSO with the addition of different equiv. of TBAF; b) The absorbance ratio (A_{302nm}/A_{380nm}) of **SHJ-2** versus F^- concentrations.

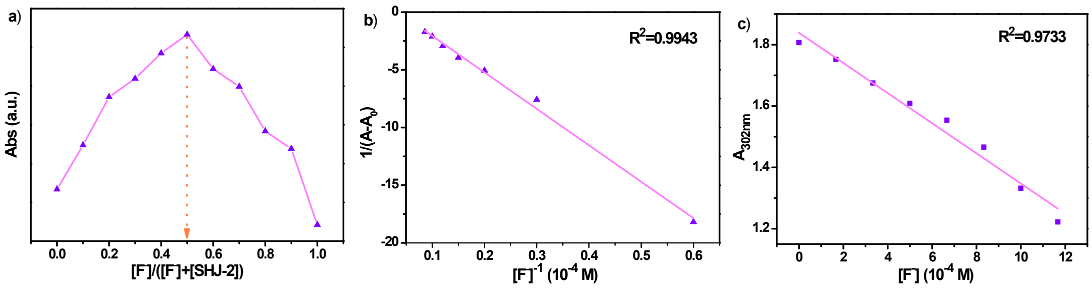

Fig. S16. a) Job's plot for complexation of **SHJ-2** with F^- anion. b) Benesi - Hildebrand plot of **SHJ-2** by UV-vis measurements. c) Absorbance of **SHJ-2** in the presence of TBAF at different concentration in DMSO.

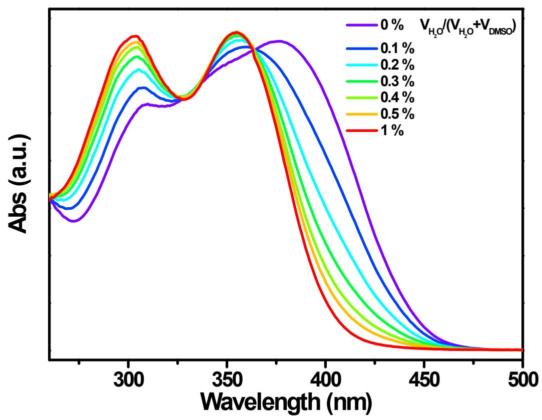

Fig. S17. Absorbance spectra of **SHJ-2** in the presence of 23.33 equivalents of TBAF in DMSO with various content of water.

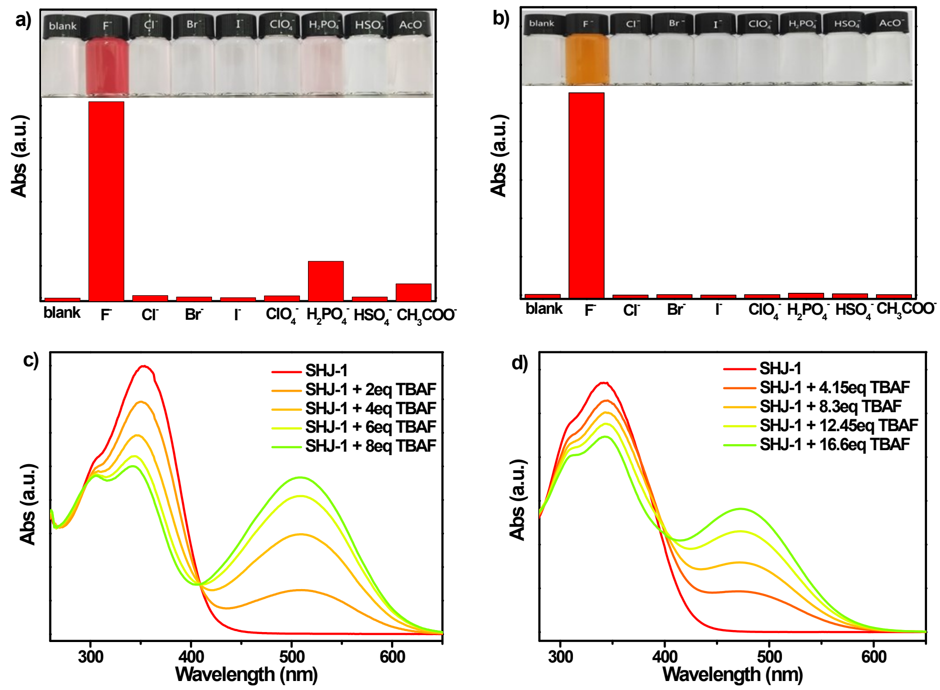

Fig. S18. The intensity of the maximum visible absorption peak of probes **SHJ-1** with the addition of 8 equiv. of various anions (as tetrabutylammonium salt) in a) DMF and b) DCM solution at room temperature. (Inset: Color changes of **SHJ-1** with the addition of 8 equiv. of various anions under ambient light). Absorption spectra of probe **SHJ-1** in c) DMF and d) DCM with the addition of different equiv. of TBAF;

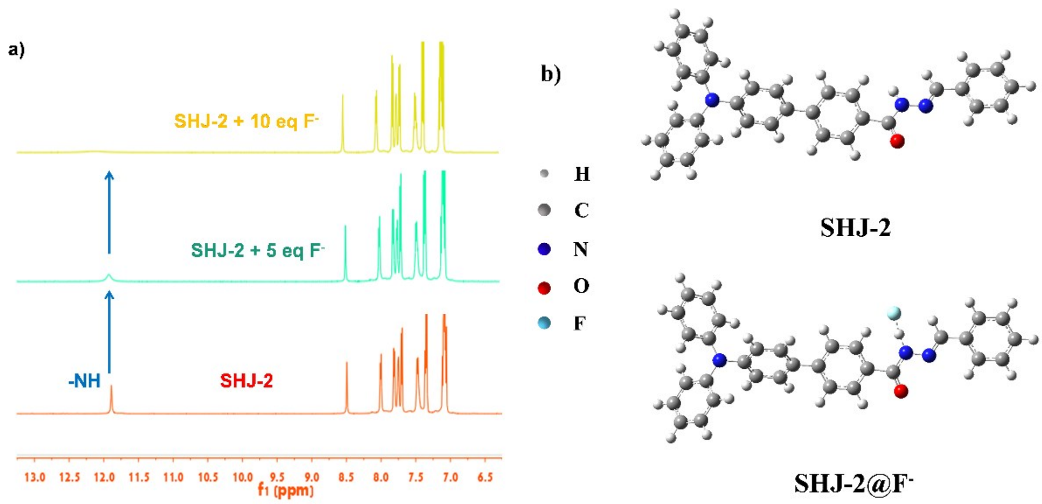

Fig. S19. a) [1]H NMR titration spectra of the probe **SHJ-2** in DMSO-d_6 in presence of differernt equivalents of TBAF; b) Optimized structures of **SHJ-2** and **SHJ-2** + F^-.

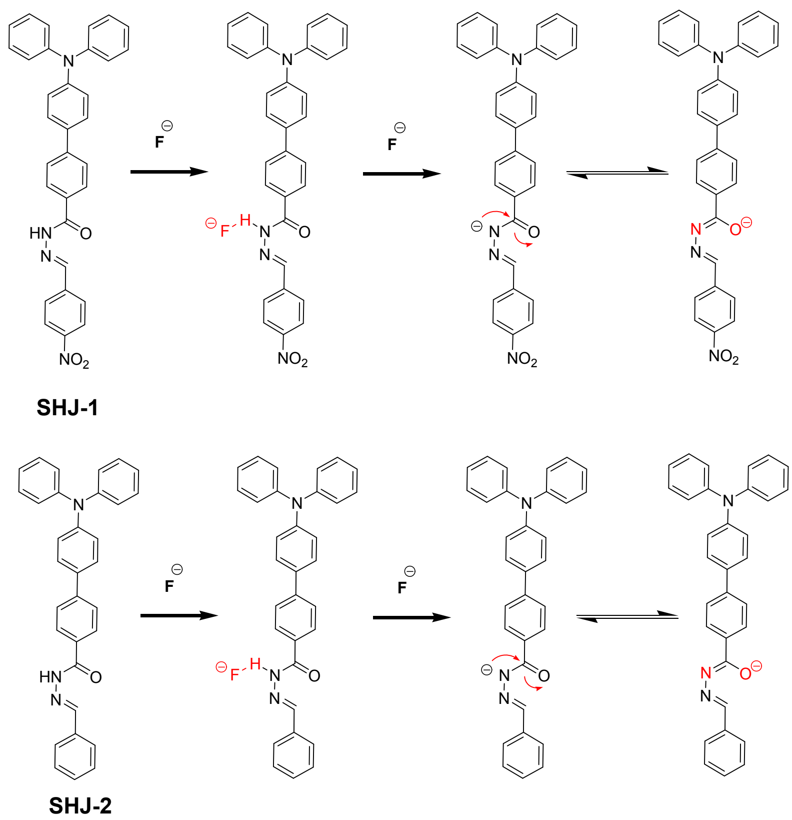

Fig. S20. A schematic of probable complex formation reaction during the fluoride sensing process

Table S1. Properties of **SHJ-1** and the reported acylhydrazone-based fluoride ion probes.

sample	λ_{max} (nm) without F^-	λ_{max} (nm) with F^-	$\Delta\lambda$ (nm)	solvent	Interference ions	[a]LOD (μM)	reference
1	370	480	110	THF	none	0.91	[41]
2	400	475	75	THF	none	-	[45]
3	404	515	111	DMSO/H_2O	none	0.55	[44]
4	293	377	84	CH_3CN	none	-	[42]
5	438	532	94	DMSO	none	0.83	[40]
6	355	500	145	DMSO	none	1.24	This work

a) The limit of detection.

Reference

1. Frisch, M. J.; Trucks, G. W.; Schlegel, H. B.; Scuseria, G. E.; Robb, M. A.; Cheeseman, J. R.; Scalmani, G.; Barone, V.; Mennucci, B.; Petersson, G. A.; Nakatsuji, H.; Caricato, M.; Li, X.; Hratchian, H. P.; Izmaylov, A. F.; Bloino, J.; Zheng, G.; Sonnenberg, J. L.; Hada, M.; Ehara, M.; Toyota, K.; Fukuda, R.; Hasegawa, J.; Ishida, M.; Nakajima, T.; Honda, Y.; Kitao, O.; Nakai, H.; Vreven, T.; Jr. Montgomery, J. A.; Peralta, J. E.; Ogliaro, F.; Bearpark, M.; Heyd, J. J.; Brothers, E.; Kudin, K. N.; Staroverov, V. N.; Kobayashi, R.; Normand, J.; Raghavachari, K.; Rendell, A.; Burant, J. C.; Iyengar, S. S.; Tomasi, J.; Cossi, M.; Rega, N.; Millam, J. M.; Klene, M.; Knox, J. E.; Cross, J. B.; Bakkem, V.; Adamo, C.; Jaramillo, J.; Gomperts, R.; Stratmann, R. E.; Yazyev, O.; Austin, A. J.; Cammi, R.; Pomelli, C.; Ochterski, J. W.; Martin, R. L.; Morokuma, K.; Farkas, O.; Foresman, J. B.; Fox, D. J. *Gaussian 16, Rev. A.03*; Gaussian, Inc.: Wallingford, CT, **2016**.